Plasma Chem Plasma Process
DOI 10.1007/s11090-012-9392-x

ORIGINAL PAPER

DBD Plasma Treatment of Titanium in O_2, N_2 and Air

S. Dahle · R. Gustus · W. Viöl · W. Maus-Friedrichs

Received: 29 February 2012 / Accepted: 11 June 2012

Abstract Dielectric Barrier Discharge plasma treatment of a titanium metal foil in oxygen, nitrogen and air under atmospheric conditions is investigated employing X-Ray Photoelectron Spectroscopy (XPS). We investigated three different reference samples and compare the results with a large number of studies on the XPS analysis of titanium compounds containing oxygen and nitrogen. The plasma treatment in all three different process gases leads to the formation of titanium dioxide films, while rather small nitrogen fractions are found after nitrogen and air plasma treatments. This finding is explained basing on plasma chemistry insight from the literature.

Keywords Dielectric barrier discharge · Titanium oxide · Titanium nitride · X-ray photoelectron spectroscopy

Introduction

Titanium and its alloys are still a current topic in different fields of scientific research such as surface or material science. The according number of papers written so far is comparatively large. Both are not least in direct relationship to the particular properties and to the variety of applications of titanium based materials.

The element titanium is known for its low density and high strength. In addition, it is corrosion resistant due to a native oxide layer formed in air. The mechanical properties and

S. Dahle · R. Gustus · W. Maus-Friedrichs (✉)
Institut für Energieforschung und Physikalische Technologien, Technische Universität Clausthal, Leibnizstrasse 4, 38678 Clausthal-Zellerfeld, Germany
e-mail: w.maus-friedrichs@pe.tu-clausthal.de

S. Dahle · W. Viöl
Fakultät für Naturwissenschaften und Technik, Hochschule für Angewandte Wissenschaft und Kunst, Von-Ossietzky-Straße 99, 37085 Göttingen, Germany

W. Maus-Friedrichs
Clausthaler Zentrum für Materialtechnik, Technische Universität Clausthal, Leibnizstrasse 4, 38678 Clausthal-Zellerfeld, Germany

Published online: 01 July 2012

the corrosive behavior can be improved by the addition of specific alloy additives like aluminum, vanadium, molybdenum etc. Thus, titanium and titanium alloys are particularly suitable in technological applications requiring light weight, stable and corrosion resistant constructions like in automobile and aerospace industry.

In the last decades, titanium oxides, especially titanium dioxide (TiO_2) have become of particular interest. Moreover, it is considered as the model system of metal oxides in surface science [1]. Several applications are associated with TiO_2, e.g., catalysis, gas sensors, white pigment, optical coatings, dielectric gate materials in MOSFET's and many more. The photocatalytic properties for example are important as a self-cleaning effect of surfaces and for purification of waste water [2]. This effect is based on the decomposition of organic molecules by reaction of radical species produced on the surface during UV irradiation. In this regard, not only single crystals but also TiO_2 layers on pure or nano-crystalline titanium are of technological interest.

For a lot of applications, the preparation of TiO_2 particles or coatings with well defined surfaces is quite important. In this context, plasma treatment is a commonly used procedure for surface modifications like etching, surface cleaning, hardening and oxidizing [3, 4]. The choice of the applied cover gas depends on the desired functionalization. Nitrogen rich gases for example are reported for nitriding thus producing high hardness surface films, oxygen rich gases will form titanium oxide layers. Most of these techniques are based on a high temperature plasma treatment under a low pressure environment. In contrast to these commonly utilized procedures, the Dielectric Barrier Discharge (DBD) technique offers the possibility to treat the surface with different cover gases at room temperature in a wide pressure range up to atmospheric conditions. The thermal influence on the sample is negligible.

While there are many studies dealing with results on titanium dioxide by means of surface science, especially X-ray Photoelectron Spectroscopy (XPS), most of these studies deal with adsorption and chemistry. Publications providing a full disclosure of binding energies or chemical shifts and full widths at half maximum (FWHM) for the elements Ti and O are rare [5]. Furthermore, the reported values for binding energies, chemical shifts, etc. are contradictory to some extend [5]. These may be due to several difficulties in quantitative interpretation of the XPS results of titanium compounds. Since some of the chemical species in complex Ti–O–N compounds are only separated by about 0.2 eV, this is far beyond the resolution reachable with commercial X-ray sources. The background substraction is difficult due to significant inelastic scattering, which gets even more complicated due to intense shake up satellites at some 13 eV above the main peaks [6]. The main structure used for detailed chemical analysis of titanium compounds is the Ti 2p, since it is the most pronounced structure of the titanium spectrum. Unfortunately, the line widths for Ti $2p_{3/2}$ and Ti $2p_{1/2}$ differ due to a different Coster-Kronig broadening, just alike most transition metals [6–9]. In addition to that, the peak areas ratio of the Ti $2p_{3/2}$ compared to the Ti $2p_{1/2}$ is commonly assumed to be 2:1, or even reported to be larger [6], while it should be about 1.94:1 when taking into account the two different photo-ionization cross sections [10].

The Ti $2p_{3/2}$ binding energies for titanium oxide compounds with Ti at common oxidation states 0, +2, +3, +4 have been reported before to be 453.9, 455.3, 457.1 and 458.7 eV, giving rise to chemical binding energy shifts of 0.0, 1.35, 3.2 and 4.8 eV, respectively [5]. The peak splitting between Ti $2p_{3/2}$ and Ti $2p_{1/2}$ has been reported to be 6.13, 5.73, 5.60 and 5.66 eV for $Ti^{(0)}$, $Ti^{(II)}$, $Ti^{(III)}$ and $Ti^{(IV)}$ oxides, respectively. Since Biesinger et al. verified their findings for Ti-apatite by comparison to a large number of references, the core level shifts of all other chemical species have been accounted to these

values. Doping of the titanium should lead to a changed Fermi energy and thus to a shift in binding energies. Nevertheless, the usage of relative binding energies between Ti $2p_{3/2}$ orbitals in different oxidation states, between Ti $2p_{3/2}$ and Ti $2p_{1/2}$ and between Ti $2p_{3/2}$ and O 1s, respectively, should always remain unaffected. Thus, the discussion of all peak positions will follow these binding energy differences. An additional oxide species has been reported for Ar^+ ion sputtered titanium oxides at about 454.2 eV for the Ti $2p_{3/2}$ peak [11, 12]. The binding energy of the Ti $2p_{3/2}$ has been reported to be 455.5 eV for TiN films grown by reactive sputter deposition [13, 14]. During the oxidation of this TiN film, an intermediate state has been reported at 457.1 eV and was proposed to belong to some titanium oxynitride species [13]. The intermediate state feature nevertheless fits very well to the reported value for Ti_2O_3 [5], which could as well be generated by nitrogen induced reduction of TiO_2. Therefore, no attempt on the differentiation of a titanium oxinitride species was made for the present study. Since the plasma treatments in different atmospheres presented later on also include some gases with perceptible water content, there might be a formation of TiH_4 or $Ti(OH)_4$ during plasma treatment due to hydrogen free radicals. The binding energy reported for a TiH_4 species which has been found on H_2-reduced TiO_2 single crystals is 454.1 eV [15]. On the comparison of the spectra of a TiO_2(001) crystal freshly introduced into a vacuum system with the spectra of the same crystal after cleaning with a scraper, a species belonging to Ti surface atoms with OH groups adsorbed was detected a Ti $2p_{3/2}$ binding energy of 457.1 eV [16], which is just the same as found for Ti_2O_3 before. All described Ti 2p values from literature reference data are summarized in Table 1.

Many of the studies specify the binding energy for the O 1s peak belonging to TiO_2 [13–15, 17–22]. Since the reported values are quite close for all of these publications with a standard deviation of 0.37 eV, the average of the binding energy values, which accounts to 529.9 eV has been used to discuss the recent results later on. The binding energy of a Ti–O–N intermediate species for the O 1s peak has been reported to amount to 531.3 eV

Table 1 Literature values of binding energy, chemical shift and doublet splitting for the Ti 2p structure in XPS

Peak	Tetrahedron	Bonding unit	Binding energy/eV	Chemical shift/eV	References
Ti $2p_{3/2}$	Ti-Ti_4	Ti	453.9	0.00	[5]
	Ti-Ti_2H_2	TiH	454.1	0.20	[15]
	Ti-Ti_3O	Ti_2O	454.2	1.10	[11, 12]
	Ti-Ti_2O_2	TiO	455.3	1.35	[5]
	Ti-N_4	TiN	455.5	1.55	[13, 14]
	Ti-TiO_3	Ti_2O_3	457.1	3.20	[5]
	Ti-O_xN_{4-x}	TiO_xN_y	457.1	3.15	[13]
	Ti-O_4	$Ti(OH)_4$	457.1	3.20	[16]
	Ti-O_4	TiO_2 amorph	458.7	4.80	[5]
Peak	Tetrahedron	Bonding unit	Binding energy/eV	Doublet splitting/eV	References
Ti $2p_{1/2}$	Ti-Ti_4	Ti	460.0	6.13	[5]
	Ti-Ti_2O_2	TiO	461.0	5.73	[5]
	Ti-TiO_3	Ti_2O_3	462.7	5.60	[5]
	Ti-O_4	TiO_2 amorph	464.4	5.66	[5]

independently by investigations on the oxidation of TiN [13], NO_2 adsorption on TiO_2(110) single crystal surfaces [17] and nitrogen incorporation into porous TiO_2 nanocolloids from alkyl ammonium compounds [20].

During the investigation of the deposited Ti layer in a magnetron-type sputter ion pump, Vesel et al. found an O 1s species at 2.2 eV above the TiO_2 bulk oxygen [14]. The same shift was found for the adsorption of the amino acid proline on rutile TiO_2 surfaces [23]. Cheung et al. reported surface adsorbed OH groups to be found at about 1.5 eV above TiO_2 bulk oxygen, i.e., 531.6 eV [18]. The same value was obtained by Xu et al. for N-doped TiO_2 powders prepared from titanium (IV) n-butoxide via hydrolization in an isopropanol—ethylamine solution subsequently oven-dried at 333 K, as well as commercial TiO_2 nano particles hydrolyzed in isopropanol and subsequently oven-dried at 333 K [21]. The adsorption of water on anatase TiO_2(101) surfaces was found to generate an O 1s species shifting between binding energy values of 534.2 and 535.2 eV, while for water on rutile only one value of 532.9 eV was found and the O 1s species for bulk TiO_2 was found at 531.0 eV [24, 25]. In contrast to that, Sham et al. found binding energy values of water adsorbed on clean as well as hydrated rutile TiO_2 surfaces shifting up to 3 eV above the O 1s species corresponding to bulk TiO_2 [16]. For a combined investigation of water sorption on TiO_2 rutile (110) single crystal face by XPS and periodic DFT, Perron et al. found adsorbed H_2O molecules 1.3 eV above TiO_2 top O groups and 2.5 eV above TiO_2 bridging O groups [26]. This yields an averaged chemical shift of 1.9 eV for the O 1s species of adsorbed OH groups relative to the O 1s peak of TiO_2 surface oxygen. A quite similar chemical shift of 1.8 eV was found during the photoreaction of acetic acid on the rutile TiO_2(011) single crystal surface for an adsorbed oxygen O 1s species proposed to belong to OH or COO groups [27]. Wang et al. found a surplus O 1s species at 1.6 eV above the bulk TiO_2 peak after the adsorption of liquid and vapor water on defective TiO_2(110) surfaces [28]. Disregarding the surplus chemical shifts found on some anatase TiO_2 systems with the origin unknown up to now, the average value for the reported chemical shifts of the O 1s peak for OH groups on TiO_2 relative to the O 1s for bulk TiO_2 amounts to 1.9 eV, with a standard derivation of less than 0.5 eV. Bilmes et al. found a peak with a chemical shift of 2.2 eV above the titanium oxide peak of the O 1s structure and proposed it to belong to physisorbed oxygen in terms of O_2^-, O_2^{2-} or O^- [29].

The N 1s structure of TiN films grown by a sputter deposition technique has been analyzed by Saha et al., finding TiN at a binding energy of 397.0 eV, surrounded by adsorbed nitrogen in the β-N state at 396.0 eV, the α-N_2 state at 397.5 eV, as well as the γ-N state at 400.0 eV for well screened and 405.0 eV for poorly screened cases [13]. Ti layers grown in magnetron-type sputter ion pumps as investigated by Vesel et al. yield a N 1s structure consisting of a dominant TiN species at 396.7 eV with a broad shoulder around 398–402 eV suggested to belong to C–N bonds, especially the formation of CN_x films [14]. After the adsorption of NO_2 on TiO_2(110), Rodriguez et al. find chemisorbed NO_3 groups with a N 1s binding energy of 407.0 eV besides the N 1s peaks of chemisorbed NO_2 at 403.5 eV and physisorbed NO_2 dimers (N_2O_4) at 406.0 eV [17]. For $TiO_{2-x}N_x$ films with (110) surface orientation grown on rutile TiO_2(110) by plasma assisted molecular beam epitaxy, Cheung et al. report N 1s binding energies of 396.0 eV for a TiN species, 400.0 eV for physisorbed N_2 and 407.0 eV for chemisorbed NO_3 [18]. Prokes et al. produced titanium oxynitride nano particles through the direct nitridation of porous TiO_2 nano colloids using alkyl ammonium compounds and found only one broad N 1s peak at 401.3 eV, suggesting it to belong to titanium oxynitride [20]. Fàbrega et al. prepared highly ordered nanoholes in a TiO_2 film by electrochemical anodization of titanium metal

foils and subsequent nitrogen incorporation by annealing in a reducing atmosphere of NH_3 or 5 % H_2 in 95 % N_2, respectively. The N 1s spectra of these films have been reported to consist of three species at binding energies of about 396, 397 and 400 eV, assigned to bulk TiN, substitutional nitrogen in TiO_2 and a γ-N state of chemisorbed molecular N_2, respectively [22]. Subsuming these references, the N 1s peak for TiN is reported at a binding energy of 396.6 eV on average with a standard deviation of about 0.5 eV. Following the references, physisorbed atoms or molecules of nitrogen should yield a N 1s peak at about 1 eV below or above the binding energy of the TiN species, respectively, while the chemisorbed oxides appear in the N 1s peak at 403.5 eV for NO_2 and 407.0 eV for NO_3. All described O 1s and N 1s values from reference data have been summarized in Table 2.

The band bending [30] and charging effects [5, 31–33] tend to become rather large on TiO_2 surfaces. Thus, the application of absolute binding energies seems to be inappropriate when fitting experimental data due to the uncertainty of the binding energy shift induced by band bending and surface charging. Some of the literature data is recorded with the experimental setup for charge compensation either by binding energy correction along to structures of some gold coating [20], or by electron dosage using a flood gun just until the adventitious carbon peak is found corresponding to given literature [5, 34]. In contrast to these approaches, taking into account relative binding energies between all species found instead of absolute values should always lead to a reasonable interpretation of experimental data.

Amongst the given references, the authors tried to collect a consistent set of values necessary for reasonable interpretation and reproducible quantitative analysis of the XPS spectra of titanium oxynitrides. Basing on values supported by most papers as reviewed by Biesinger et al. [5], data from charge corrected measurements on reference samples as opposed to DFT calculations have been adjoined. Reference data have been completed by values averaged from independent investigations of several applied samples where standard deviations are satisfyingly small. The fitting procedures presented later on are based on these results, i.e., the chemical shifts as well as binding energy differences between different atoms for the bonding units presented above. A verification of these procedures is

Table 2 Literature values of binding energy and chemical shift for the O 1s and N 1s structures in XPS

Peak	Bonding unit	Binding energy/eV	Chemical shift/eV	References
O 1s	TiO_2	529.9	0.00	[13–15, 17, 18, 20–22]
	TiO_xN_{4-x}	531.3	1.40	[13]
	$Ti(OH)_4$	531.8	1.90	[14, 18, 21, 22, 24, 25, 27–29]

Peak	Bonding unit or state	Binding energy/eV	Chemical shift/eV	References
N 1s	β-N	396.0	−0.60	[13, 14, 18]
	TiN	396.6	0.00	[13, 14, 22]
	α-N_2	397.3	0.65	[13, 22]
	CN_x	400.0	3.40	[14]
	γ-N	400.0	3.40	[13]
	NO_2	403.5	6.90	[17]
	N_2O_4 (NO_2-Dimer)	406.0	9.40	[17]
	NO_3	407.0	10.40	[17, 18]

given by maintaining results similar to given references for standard reference samples without any constraints during analysis. Afterwards, a plasma treatment of titanium substrates is presented employing binding energy differences as summarized in Tables 1 and 2.

The tetrahedron notation used in Table 1 as well as during the discussion of our results is implemented analogous to the notation of Cova et al. for silicon oxynitride films [34]. Since there are several bonds inducing equal oxidation states at the titanium atoms, the notation of oxidation states is not unique and thus not capable for discussions. The different models that are commonly used to describe the structure of amorphous nonstoichiometric alloys are the random bonding model (RBM) and the random mixture model (RMM) [35–38]. According to silicon-centered tetrahedrons considered by Cova et al., the discussion of titanium species will be held considering titanium-centered tetrahedrons. Silicon films grown by low pressure chemical vapor deposition techniques have been found difficult to analyze with the strict models RBM and RMM. Thus, a more general model has been proposed to be useful especially for films grown under highly nonequilibrium conditions, e.g., plasma-assisted chemical vapor deposition techniques. The new approach proposed by Cova et al., the extended random mixture model (ERMM) demands a well choice of the most adequate tetrahedral structures among all possible candidates. After exclusion of unlikely tetrahedrons, the remaining units have to be considered during the numerical fitting of XPS spectra, using binding energies gained through calculations as well as reference spectra of pure standard samples. Finally, the fractions of the total number of atoms belonging to that species can be calculated taking into account the stoichiometry coefficient for the species related to the particular tetrahedron [35].

Experimental Details

An ultra high vacuum apparatus with a base pressure of 5×10^{-11} hPa is used to carry out the experiments [39]. All measurements were performed at room temperature.

XPS is performed using a hemispherical analyzer (VSW HA100) in combination with a commercial non-monochromatic X-ray source (Specs RQ20/38C). During measurements, X-ray photons irradiate the surface under an angle of 80° to the surface normal, illuminating a spot with a diameter of several mm. For all measurements presented here the Al K_α line (photon energy 1,486.6 eV) is used. Electrons are recorded by the hemispherical analyzer with an energy resolution of 1.1 eV emitted under an angle of 10° to the surface normal. All XPS spectra are displayed as a function of binding energy with respect to the Fermi level.

For quantitative XPS analysis, photoelectron peak areas are calculated via mathematical fitting with Gauss-type profiles using OriginPro 7G including the PFM fitting module, which applies Levenberg–Marquardt algorithms to achieve the best agreement possible between experimental data and fit. To optimize our fitting procedure, Voigt-profiles have been applied to various oxidic and metallic systems previously, but for most systems the Lorentzian contribution converges to zero. Therefore, all XPS peaks are fitted with Gaussian shapes. The background correction was done by the combination of a Shirley-type background correction with the high binding energy site limit at the maximum of the first shake up satellite and a subsequent linear subtraction. Although it has been shown that constant tail background approaches yield best results, its advantage is negligible due to the lack of pure standard spectra [6]. Fitting the Ti 2p structure was performed constraining chemical shifts and core level splittings as discussed in the introduction and summarized in

Table 1. The O 1s structure has been fitted using the full width at half maximum (FWHM) gained from the spectra of a cleaned TiO_2 single crystal surface as presented amongst the results and the chemical shift of 1.9 eV for adsorbed OH groups. Photoelectric cross sections as calculated by Scofield [10] with asymmetry factors after Powell and Jablonski [40], taking into account asymmetry parameters after Reilman et al. [41] and Jablonski [42] as well as inelastic mean free paths from the NIST database [43] (using the database of Tanuma, Powell and Penn for elementary contributions and the TPP-2M equation for molecules) as well as the energy dependent transmission function of our hemispherical analyzer are taken into account when calculating stoichiometries. The transmission function of the analyzer was estimated following Hesse et al. by reference measurements on gold, silver, copper and germanium [44] to be $T(E_{kin}) = 0.6736 - 0.5855\ \varepsilon + 2.677\ \varepsilon^2 - 1.8076\ \varepsilon^3 - 0.3281\ \varepsilon^4 + 2.1812\ (E_{kin})^{-0.275}$ with $\varepsilon = (E_{kin} - 1{,}000\ \text{eV})/1{,}000\ \text{eV}$ [45].

Plasma treatments have been carried out employing a dielectric barrier discharge. The plasma source is mounted to a preparation chamber with a base pressure of 5×10^{-8} hPa which is connected directly to the UHV recipient via a common transfer system and has been described elsewhere [46]. An alternating high voltage pulse generator with a pulse duration of 0.6 µs and a pulse repetition rate of 10 kHz is connected to the dielectric isolated electrode, while the sample forms the grounded counter electrode. The discharge gap is set to about 1 mm and the discharge area is about 2 cm^2. During the plasma treatment, a voltage of 11 kV (peak) is measured. The high voltage supply delivers a power of 2 W, the plasma power density can be calculated to 1 W/cm^2 and with a plasma treatment time of 60 s, an energy density of 60 J/cm^2 is applied to the sample. The increase of the sample temperature during the plasma treatment does not exceed 10 K [47]. O_2 (Linde Gas, 99.995 %), N_2 (Linde Gas, 99.8 %) and ambient atmospheric air are offered via backfilling the chamber using a bakeable leak valve. The gas line is evacuated and can be heated in order to ensure cleanness. A quadrupole mass spectrometer (Balzers QMS112A) is used to monitor the partial pressure of the reactive gases simultaneously during all experiments. The titanium foil substrate (Alfa Aesar, 99.99+%) used for plasma treatments later on, a TiO_2(110) single crystal (MATEK company), as well as a chip cut out of a titanium sputter target (Alfa Aesar, 99.7 %) have been cleaned by heating to above 600 °C prior to experiments.

Results

In this section, the XPS results for three titanium references and the three plasma treatments on the titanium foil are presented. As references we investigated a TiO_2 single crystal and two different pure titanium substrates. These were previously heated to at least 600 °C to remove surface contaminations like adsorbed oxygen and carbon. The obtained values for peak widths (FWHM) were subsequently used as references to analyze the spectra of the plasma treated titanium foil, while the binding energy differences and the peak area ratios in comparison with the literature data summarized in Tables 1 and 2 serve as verification of our background subtraction and peak fitting procedures.

Pure Titanium and Titanium Oxide Samples

Figure 1 shows the XPS survey spectra of the titanium foil, the titanium sputter target and the TiO_2 single crystal. All samples exhibit the well-known elemental peaks of titanium corresponding to the Ti 2p, Ti 2s, Ti 3s and Ti 3p orbitals. In addition, the Ti LMM Auger

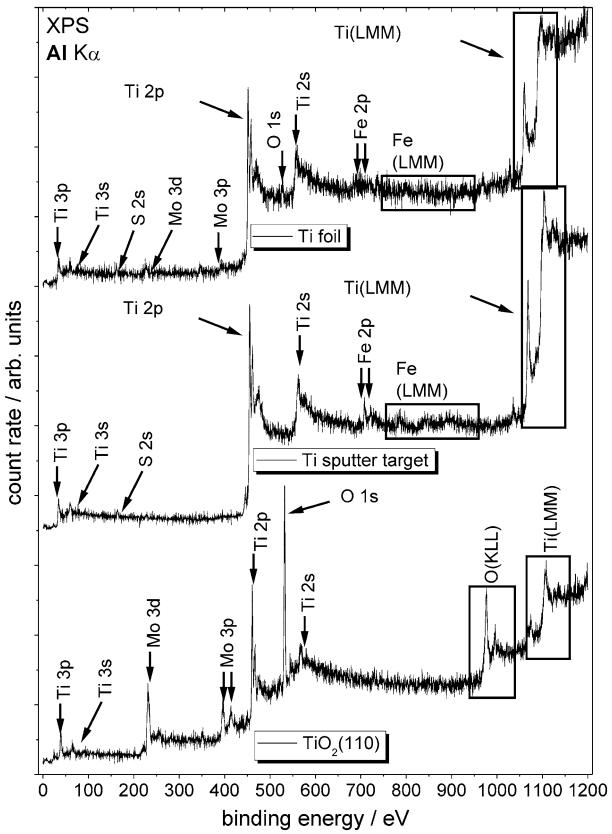

Fig. 1 XPS survey spectra of a cleaned Ti foil, a Ti sputter target chip and a TiO_2(110) single crystal surface

transition is also visible. The titanium foil and the titanium sputter target show dopants like sulphur (S 2s) and iron (Fe 2p, Fe LMM), which probably migrate from the bulk to the surface during thermal annealing and further oxygen (O 1s) for some extent, which might be due to the sample holder. Besides these, the spectrum of the sputter target additionally contains two peaks of molybdenum (Mo 3p, Mo 3d) which originate from the sample holder and which are not part of the sample. Peaks related to carbon impurities could not be found on any sample, implying that this contaminant was totally removed by the cleaning procedure. The total stoichiometry of the the titanium foil consists of 77.9 % Ti, 8.6 % O, 13.5 % S and less than 1.5 % Fe. The titanium sputter target contains 77.7 % Ti, 4.6 % O, 11.6 % S and 6.1 % Fe. Additionally, the XPS survey spectrum of the TiO_2 single crystal shows oxygen, indicated by the emission of the O 1s orbital and the O KLL Auger transition. Besides these, no other peaks referring to any surface contaminations could be found. The molybdenum still originates from the sample holder. In total the stoichiometry of the TiO_2 single crystal shows 26.8 % Ti and 73.2 % O, thus the resulting O:Ti ratio amounts to 2.7. This elevated ratio should mainly be due to geometric effects. Since the TiO_2 surfaces are typically oxygen terminated, the assumption of a homogeneous distribution for calculating stoichiometries is not the case. This alignment leads to an overestimation of the oxygen fraction relative to the titanium. Nevertheless, the obtained value for oxygen terminated TiO_2 surfaces can be used for comparison during interpretation of

Table 3 Stoichiometries of all samples calculated from peak intensities in the XPS survey spectra as displayed in Figs. 1 and 3

	$n\%_{Ti}$	$n\%_{O}$	$n\%_{N}$	$n\%_{C}$	$n\%_{S}$	$n\%_{Fe}$
Sample						
Ti foil	77.9 %	8.6 %	0.0 %	0.0 %	13.5 %	<1.5 %
Sputter target	77.7 %	4.6 %	0.0 %	0.0 %	11.6 %	6.1 %
TiO_2	26.8 %	73.2 %	0.0 %	0.0 %	0.0 %	0.0 %
Treatment of Ti foil						
O_2-plasma	30.9 %	69.1 %	0.0 %	0.0 %	0.0 %	0.0 %
N_2-plasma	23.9 %	69.5 %	1.1 %	5.5 %	0.0 %	0.0 %
Air-plasma	23.2 %	69.8 %	1.4 %	5.6 %	0.0 %	0.0 %

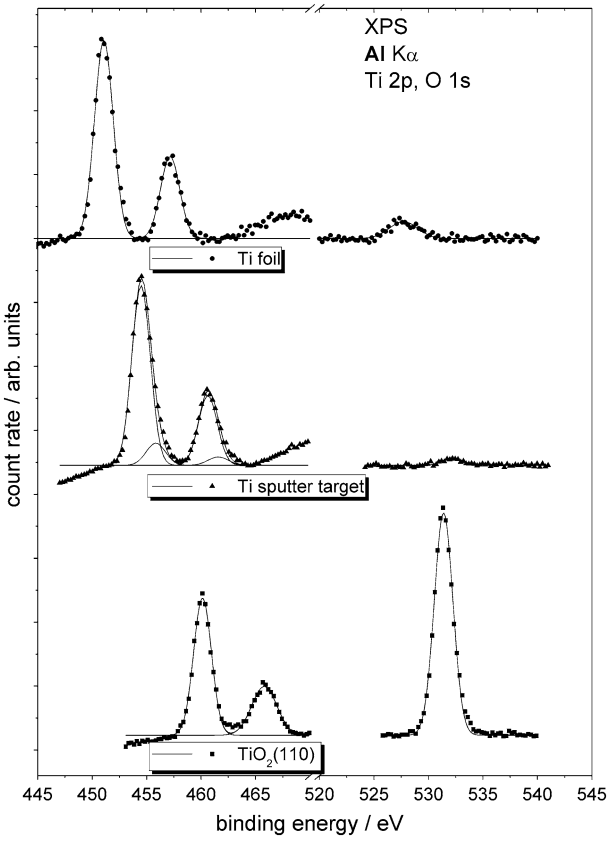

Fig. 2 XPS detail spectra of the Ti 2p and O 1 s regions of a cleaned Ti foil, a Ti sputter target chip and a TiO_2(110) single crystal surface

the plasma treated samples' results. The stoichiometries of the three reference samples are further summarized in Table 3.

The Ti 2p and O1 s detail spectra are depicted in Fig. 2. The Ti 2p structure of the titanium foil could be fitted with only one peak doublet which can be assigned to metallic titanium (Ti-Ti_4). For the Ti sputter target, a shake-up structure around 470 eV is visible due to inelastical scattered electrons emitted from the Ti 2p orbitals. The small amount of

Table 4 Summarized XPS results from the Ti 2p region as displayed in Figs. 2 and 4

	Peak	Binding energy/eV	FWHM/eV	Area/arb. units	Correlation
Sample					
Ti foil	Ti $2p_{3/2}$	451.1	2.03	334.0	Ti-Ti_4
	Ti $2p_{1/2}$	457.2	2.08	141.4	Ti-Ti_4
Ti sputter target	Ti $2p_{3/2}$	454.5	1.99	1105.7	Ti-Ti_4
		455.8	2.08	143.2	Ti-Ti_2O_2
	Ti $2p_{1/2}$	460.6	2.05	438.7	Ti-Ti_4
		461.6	2.19	56.6	Ti-Ti_2O_2
TiO_2(110)	Ti $2p_{3/2}$	460.1	1.93	522.5	Ti-O_4
	Ti $2p_{1/2}$	465.8	2.73	262.7	Ti-O_4
Treatment of Ti foil					
O_2-plasma	Ti $2p_{3/2}$	459.5	2.02	590.5	Ti-O_4
	Ti $2p_{1/2}$	465.2	2.61	256.3	Ti-O_4
N_2-plasma	Ti $2p_{3/2}$	459.4	2.04	572.7	Ti-O_4
	Ti $2p_{1/2}$	465.1	2.66	241.2	Ti-O_4
Air-plasma	Ti $2p_{3/2}$	459.7	2.01	572.5	Ti-O_4
	Ti $2p_{1/2}$	465.4	2.58	242.2	Ti-O_4

Table 5 Summarized XPS results from the O 1s region as displayed in Figs. 2 and 5

	Binding energy/eV	FWHM/eV	Relative intensity	Correlation
Sample				
Ti foil	527.7	3.04	1.00	Mount
Ti sputter target	532.2	2.28	1.00	Mount
TiO_2(110)	531.4	2.02	1.00	Ti–O
Treatment of Ti foil				
O_2-plasma	531.0	2.02	0.81	Ti–O
	532.9	2.64	0.19	Physisorbed OH or O_2
N_2-plasma	530.9	2.06	0.87	Ti–O
	532.8	1.98	0.13	Physisorbed OH or O_2
Air-plasma	531.2	2.07	0.82	Ti–O
	533.1	2.45	0.18	Physisorbed OH or O_2

oxygen is therefore not bound to titanium, but probably originates from oxygen adsorbed on the sample holder. The sputter target shows two Ti 2p species referring to metallic titanium (Ti-Ti_4) and titanium-(II)-oxide (Ti-Ti_2O_2) at higher binding energy, indicating that not all oxygen bonded species on the sample could be removed during the cleaning procedure. The Ti 2p and O 1s spectra of the TiO_2 single crystal both contain one single species, respectively, which can be assigned to titanium oxide species. The values for the binding energies, energy widths (FWHM), peak areas and peak correlations are summarized in Tables 4 and 5. The XPS structures do not follow the absolute binding energy positions from the literature, but show some shifts due to the different doping and maybe some charging effects. Nevertheless, the relative positions of the Ti 2p—species and the O 1s peak fit very well and thus validate the analysis and interpretation.

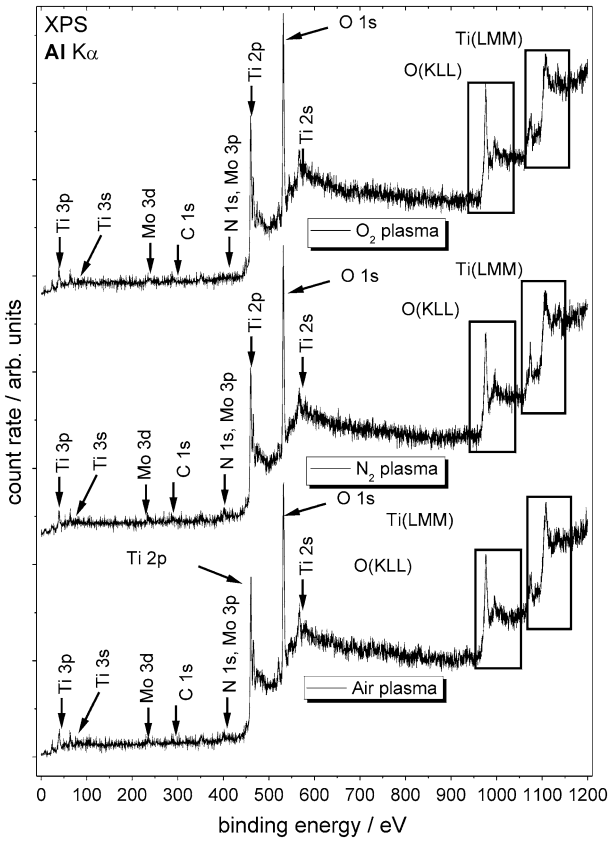

Fig. 3 XPS survey spectra of a cleaned Ti foil after DBD plasma treatment in O_2, N_2 and air, respectively

Plasma-Treatment

The survey spectra of the titanium foil plasma treated for 60 s in 1,000 mbar of air, 200 mbar of nitrogen and 200 mbar of oxygen are shown Fig. 3. Besides the well-known elemental peaks of titanium (Ti 2s, Ti 2p, Ti 3s, Ti 3p), the spectra show distinct peaks of oxygen (O 1s, O KLL), due to an oxygen incorporation during plasma treatment. In contrast to that, sulphur (S 2s) is no longer detectable. In the case of air and nitrogen plasma, a small amount of nitrogen (N 1s) and carbon (C 1s) is visible, respectively. The stoichiometry results for the three plasma treatments are summarized in Table 3.

The Ti 2p detail spectra in Fig. 4 could be fitted with one species, assigned to titanium dioxide (Ti-O_4). Additional titanium species such as metallic titanium could not be found. It can therefore be concluded that the surface is completely oxidized at least up to the information depth of XPS not only when using oxygen containing process gases like O_2 or air, but also for pure N_2 with less than 0.2 % of gaseous contaminants.

The O 1s spectra of the three plasma treatments are shown in Fig. 5. Each spectrum is fitted with two peaks, the main peak belonging to TiO_2 and the second one at higher binding energy most probably representing physisorbed OH groups, while physisorbed oxygen would appear at similar binding energy [30].

The detail spectra of the N 1s orbital regarding to the nitrogen and air plasma are presented in Fig. 6. Concerning the binding energies determined from the spectra we

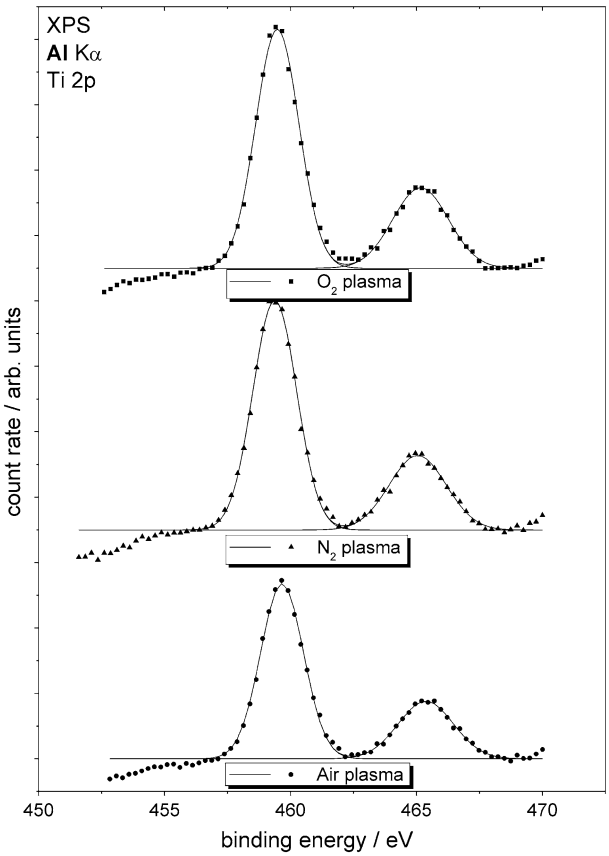

Fig. 4 XPS detail spectra of the Ti 2p region of a cleaned Ti foil after DBD plasma treatment in O_2, N_2 and air, respectively

conclude that both peaks originate from titanium nitride (Ti-N_4). During the O_2 DBD treatment no N formation is observed at all up to our XPS detection limit.

As mentioned, an unsignificantly small amount of carbon is also detectable. Figure 7 shows the C 1s detail spectra for the different plasma treatments. Most probably the carbon refers to adventitious carbon and is not at least bonded to titanium. All XPS results from this section are summarized in Tables 4, 5, 6 and 7 as divided into Si 2p, O 1s, N 1s and C 1s peak.

Discussion

The results for the reference samples discussed in Sect. 3.1 clearly verify the literature data as discussed in Sect. 1 and summarized in Tables 1 and 2, even though purity was only gained to a very limited extend due to enrichment of doping agents at the surface during the in-vacuo cleaning procedure. For the TiO_2(110) single crystal almost no additional species have been found, but a O:Ti ratio of 2.7 indicates surplus oxygen which is probably due to the oxygen terminated surface and physisorbed OH groups, but could as well belong to physisorbed oxygen [30]. Binding energy differences between the metallic Ti $2p_{3/2}$ peak (Ti-Ti_4) and the O 1s peak belonging to TiO_2 have been found to be 76.6 and 77.7 eV for

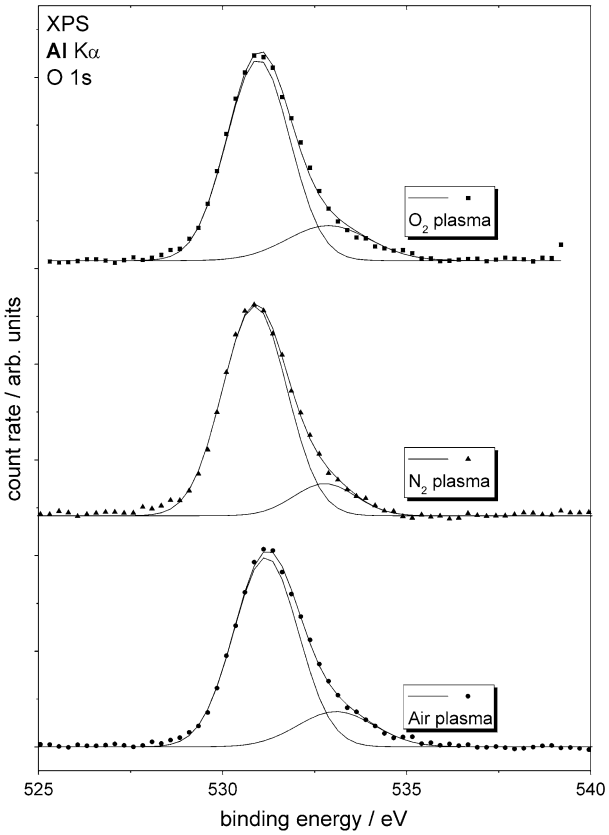

Fig. 5 XPS detail spectra of the O 1s region of a cleaned Ti foil after DBD plasma treatment in O_2, N_2 and air, respectively

the Ti foil and the Ti sputter target, respectively, whereas literature data demanded 76.0 eV (see Tables 1, 2). The Ti $2p_{3/2}$–Ti $2p_{1/2}$ doublet splitting of 6.13 eV for the Ti-Ti_4 species and 5.73 eV for the Ti-Ti_2O_2 species according to literature was constrained for the Ti sputter target, giving rise to the same FWHM as found without declaring any constraints at the results of the Ti foil. Furthermore, a Ti 2p doublet splitting of 6.08 eV was gained, reproducing the literature value quite well. The quantitative analysis for the TiO_2(110) single crystal yielded a binding energy difference between Ti $2p_{3/2}$ and O 1s of 71.26 eV, which is in good agreement to the literature value of 71.20 eV. Furthermore, the Ti 2p doublet splitting of 5.67 eV fits very well to the literature value of 5.66 eV.

Each of the Ti foils plasma treated in O_2, N_2 and air yields only one peak doublet in the Ti 2p region with a doublet splitting of 5.69, 5.68 and 5.71 eV, respectively, thus resembling the literature value for the Ti-O_4 of 5.66 eV quite well. The FWHMs are also reproduced well for all three samples, as well as the binding energy differences between Ti $2p_{3/2}$ and the main O 1s species which is assumed to be corresponding to TiO_2. These binding energy differences amount to 71.50, 71.53 and 71.52 eV for the Ti foil treated in an O_2 plasma, N_2 plasma or air plasma, respectively. The literature value of 71.20 eV is not far away from this, which suggests that the interpretation is quite consistent, since no constraints have been used at all during the fitting procedures. Even though only one species could clearly be distinguished in the Ti 2p region, the binding energy differences between the Ti $2p_{3/2}$ peak and the N 1s peak of 56.07 eV for the N_2 plasma treated and

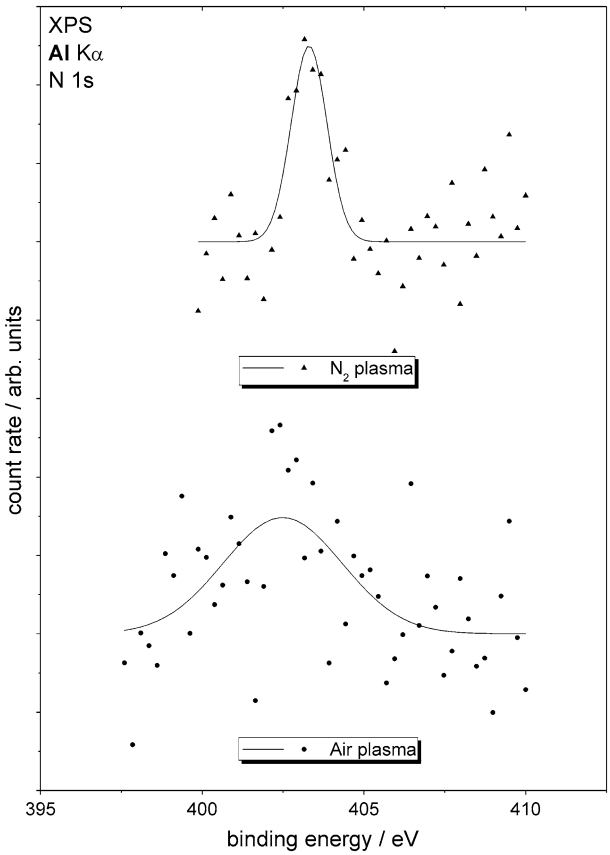

Fig. 6 XPS detail spectra of the N 1s region of a cleaned Ti foil after DBD plasma treatment in N_2 and air, respectively

57.16 eV for the air plasma treated sample are very close to the value of 57.30 eV for the N 1s peak of TiN versus the Ti-Ti_4 peak of the Ti $2p_{3/2}$ structure. This indicates that all nitrogen is chemisorbed at the titanium surface for the N_2 plasma treated foil, while no interaction with the oxygen atoms takes place, since oxynitrides should yield notably larger binding energy differences according to the literature values. This is rather surprising, since the used N_2 had less than 1 % contaminants, mainly water. Since there was no other oxygen source present during the plasma treatment, this has to be the origin of the incorporated oxygen. At some 10^{-1} hPa contaminant vapor partial pressure, the resulting dosage of oxygen radicals could be sufficient for these findings. The FWHM of the air plasma treated Ti foil foretells a remarkable broadened N 1s peak, indicating the formation of oxynitrides. Due to the low signal corresponding to a very small fraction, this can not be evaluated with reliable certainty from the results. Therefore, the assumption that nitric oxides are present gives an impression of the maximum amount of nitrogen that could be present. This amount might be even smaller in the case of the air plasma treated sample. Nonetheless, the fraction of nitrogen is well below 1.5 %, thus mainly TiO_2 seems to be formed even during N_2 and air plasma treatments. A surplus peak in the O 1s region of all three plasma treated samples at 1.9 eV above the TiO_2 peak most probably suggests OH groups adsorbed at the surface from water contamination of the process gas, while physisorbed oxygen would be found at similar binding energies [30]. Since several minutes of

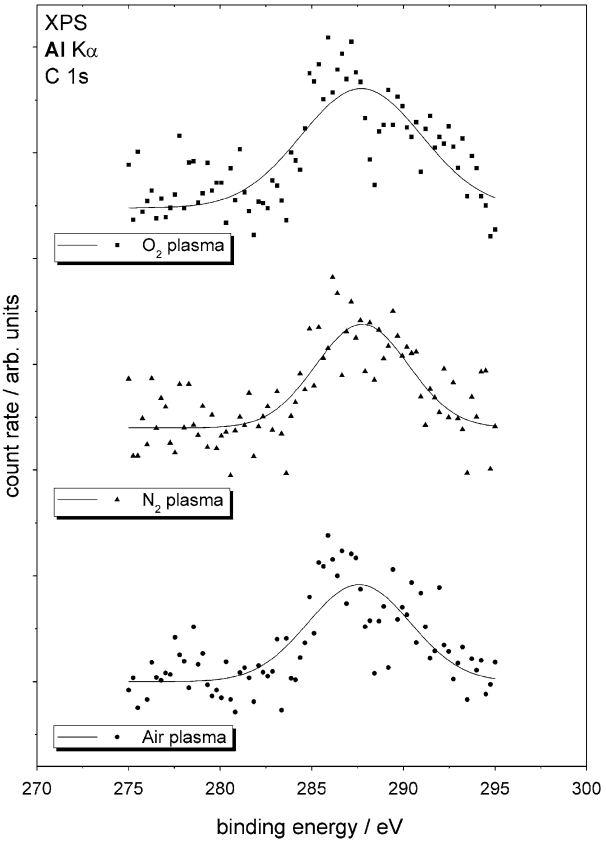

Fig. 7 XPS detail spectra of the C 1s region of a cleaned Ti foil after DBD plasma treatment in O_2, N_2 and air, respectively

Table 6 Summarized XPS results from the N 1s region as displayed in Fig. 6

Sample	Binding energy/eV	FWHM/eV	Relative intensity	Correlation
O_2-plasma	–	–	–	–
N_2-plasma	403.3	1.3	1.00	TiN
Air-plasma	402.5	4.3	1.00	TiN

Table 7 Summarized XPS results from the N 1s region as displayed in Fig. 7

Treatment of Ti foil	Binding energy/eV	FWHM/eV	Relative intensity	Correlation
O_2-plasma	287.7	7.75	1.00	Adventitious carbon
N_2-plasma	287.8	5.94	1.00	Adventitious carbon
Air-plasma	287.6	6.59	1.00	Adventitious carbon

pumping time decayed between plasma treatment and transfer into the UHV chamber, less than 1 ppm water contamination in the process gas would have been sufficient for this amount of adsorbed OH groups. While over-stoichiometric amounts of oxygen at the N_2 plasma and air plasma treated foil might mainly be due to the adventitious carbon that is

found with a stoichiometric fraction of about 5.5 %, not all of the surplus oxygen may be explained in this way. These results are consistent with the O_2 plasma treated Ti foil as well as the TiO_2(110) single crystal surface.

The plasma treated Ti foils with the process gases N_2 as well as atmospheric air both yield a nitrogen fraction of less than 1.5 %. This indicates that even very small oxygen fractions within the process gas are sufficient to inhibit nitride formation in favor of oxide formation, i.e., for the used nitrogen gas with an oxygen fraction of less than 0.2 %. One reason for this disparity in plasma reactivities between oxygen and nitrogen might be found in the relaxation processes. Metastable excited nitrogen molecules occupying the $A^3\Sigma_u^-$ state have been found to relax during inelastic collisions with oxygen molecules at ground state $X^3\Sigma_g^+$ under the formation of two oxygen radicals [48, 49]. Additionally, this metastable state of the nitrogen molecule has been proposed to remain after relaxation from the next 4 excited states above [50, 51]. This process explains very well the enhanced oxygen radical formation for plasma discharges with nitrogen containing process gases and the enhanced reactivities of small fractions of oxygen in a nitrogen process gas, which have been found to prevail the reactivity of the nitrogen itself.

Summary

The analysis of three different titanium substrate references has been shown to be in great compliance with a large number of publications. Basing on these data, the formation of TiO_2 was shown for Ti foils plasma treated in pure O_2 and N_2, as well as atmospheric air. Even though this seems surprising at first, the low nitrogen fractions of less than 1.5 % after air plasma treatment and even after N_2 plasma treatment may possible be explained according to a nitrogen relaxation through oxygen radical generation. Thus, plasma treatment of titanium in air at atmospheric conditions is proposed as useful technique for cleaning and controlled oxidation of titanium surfaces. Especially, the controlled oxidation even in nitrogen-rich atmospheres with low oxygen content is much easier for passivation purposes than present methods. Furthermore, its great advantage is the concurrent surface cleaning from atmospheric contaminants as adventitious carbon species or adsorbed aerosols.

Acknowledgments We gratefully acknowledge the financial support by the Deutsche Forschungsgemeinschaft (DFG) under project numbers MA1893/18-1 and VI359/9-1.

References

1. Diebold U (2003) Surf Sci Rep 48:53–229
2. Mills A, Davies HR, Worsley D (1993) Chem Soc Rev 22:417–425
3. El-Hossary FM, Negm NZ, Khalil SM, Raaif M (2005) Appl Surf Sci 239:142–153
4. Burns GP, Baldwin IS, Hastings MP, Wilkes JG (1989) J Appl Phys 66:2320–2324
5. Biesinger MC, Lau LWM, Gerson AR, Smart RSC (2010) Appl Surf Sci 257:887–898
6. Robinson KS, Sherwood PMA (1984) Surf Interf Anal 6:261–266
7. de Siervo A, Landers R, de Castro SGC, Kleiman GG (1998) J Electron Spectr Relat Phenom 88–91:429–433
8. Nyholm R, Martensson N, Lebugle A, Axelsson U (1981) J Phys F Metal Phys 11:1727–1733
9. Yarzhemsky VG, Reich T, Chernysheva LV (1992) J Electron Spectr Relat Phenom 58:67–73
10. Scofield JH (1976) J Electron Spectrosc Relat Phenom 8:129–137
11. Idriss H, Kim KS, Barteau MA (1992) Surf Sci 262:113–127

12. Idriss H, Barteau MA (1994) Catal Lett 26:123–139
13. Saha NC, Tompkins HG (1992) J Appl Phys 72:3072–3079
14. Vesel A, Mozetic M, Kovac J, Zalar A (2006) Appl Surf Sci 253:2941–2946
15. Sayers CN, Armstrong NR (1978) Surf Sci 77:301–320
16. Sham TK, Lazarus MS (1979) Chem Phys Lett 68:426–432
17. Rodriguez JA, Jirsak T, Liu G, Hrbek J, Dvorak J, Maiti A (2001) J Am Chem Soc 123:9597–9605
18. Cheung SH, Nachimuthu P, Joly AG, Engelhard MH, Bowman MK, Chambers SA (2007) Surf Sci 601:1754–1762
19. Chen X, Lou Y, Samia ACS, Burda C, Gole JL (2005) Adv Funct Mater 15:41–49
20. Prokes SM, Gole JL, Chen X, Burda C, Carlos WE (2005) Adv Funct Mater 15:161–167
21. Xu J, Ao Y, Fu D, Yuan C (2008) J Cryst Growth 310:4319–4324
22. Fàbrega C, Andreu T, Güell T, Prades JD, Estradé S, Rebled JM, Peiró F, Morante JR (2011) Nanotechnology 22:235403
23. Fleming GJ, Adib K, Rodriguez JA, Barteau MA, White JM, Idriss H (2008) Surf Sci 602:2029–2038
24. Herman GS, Dohnálek Z, Ruzycki N, Diebold U (2003) J Phys Chem B 107:2788–2795
25. Hugenschmidt MB, Gamble L, Campbell CT (1994) Surf Sci 302:329–340
26. Perron H, Vandenborre J, Domain C, Drot T, Roques J, Simoni R, Ehrhardt JJ, Catalette H (2007) Surf Sci 601:518–527
27. Quah EL, Wilson JN, Idriss H (2010) Langmuir 26:6411–6417
28. Wang LQ, Baer DR, Engelhard MH, Shultz AN (1995) Surf Sci 344:237–250
29. Bilmes SA, Mandelbaum P, Alvarez F, Victoria NM (2000) J Phys Chem B 104:9851–9858
30. Campbell CT (1997) Surf Sci Rep 27:1–111
31. McCafferty E, Wightman JP (1999) Appl Surf Sci 143:92–100
32. Massaro C, Rotolo P, De Riccardis F, Milella E, Napoli A, Wieland M, Textor M, Spencor ND, Brunette DM (2002) J Mater Sci Mater Med 13:535–548
33. Hashimoto S, Tanaka A, Murata A, Sukarada T (2004) Surf Sci 556:22–32
34. Cova P, Poulin S, Grenier O, Masut RA (2005) J Appl Phys 97:073518
35. Gritsenko VA, Kwok RWM, Wong H, Xu JB (2002) J Non-Cryst Solids 297:96–101
36. Sassella A (1993) Phys Rev B 48:14208–14215
37. Hasegawa S, He L, Inokuma T, Kurata Y (1992) Phys Rev B 46:12478–12484
38. Yin Z, Smith FW (1990) Phys Rev B 42:3658–3665
39. Frerichs M, Voigts F, Maus-Friedrichs W (2006) Appl Surf Sci 253:950–958
40. Powell C, Jablonski A (2010) J Electron Spectrosc Relat Phenom 178:331–346
41. Reilman RF, Msezane A, Manson ST (1976) J Electron Spectrosc Relat Phenom 8:389–394
42. Jablonski A (1995) Surf Interf Anal 23:29–37
43. National Institute of Standards and Technology Electron Inelastic-Mean-Free-Path Database 1.2. http://www.nist.gov/srd/nist71.cfm. Accessed 29 Feb 2012
44. Hesse R, Streubel P, und Szargan R (2005) Surf Interf Anal 37:589–607
45. Voigts F (2010) PHD thesis at the TU Clausthal
46. Wegewitz L, Dahle S, Höfft O, Voigts F, Viöl W, Endres F, Maus-Friedrichs W (2011) J Appl Phys 110:033302
47. Kogelschatz U (2003) Plasma Chem Plasma Phys 23:1–46
48. Trompeter FJ (2001) PHD thesis at the RWTH Aachen
49. Penetrante BM, Hsiao MC, Bardsley JN, Merritt BT, Vogtlin GE, Kuthi A, Burkhart CP, Bayless JR (1997) Plasma Sources Sci Technol 6:251–259
50. Aleksandrov NL, Bazelyan EM, Kochetov IV, Dyatko NA (1997) J Phys D Appl Phys 30:1616–1624
51. Piper LG, Caledonia GE, Kennealy JP (1981) J Chem Phys 74:2888–2895